

COMMUNICATION

[View Article Online](#)
[View Journal](#) | [View Issue](#)



Cite this: *Energy Environ. Sci.*, 2016, 9, 3666

Received 6th September 2016,
Accepted 25th October 2016

DOI: 10.1039/c6ee02604d

www.rsc.org/ees

Stabilizing high voltage LiCoO_2 cathode in aqueous electrolyte with interphase-forming additive[†]

Fei Wang,^a Yuxiao Lin,^b Liumin Suo,^c Xiulin Fan,^a Tao Gao,^a Chongyin Yang,^a Fudong Han,^a Yue Qi,^b Kang Xu^d and Chunsheng Wang^{*a}

Aqueous lithium ion batteries (ALIBs) receive increasing attention due to their intrinsic non-flammable nature. Their practical application, however, has been prevented by the poor electrochemical stability of aqueous electrolytes, which severely restricts the choice of anode and cathode materials for such batteries and leads to low energy densities. It has been demonstrated that "water-in-salt" electrolytes can provide an expanded voltage window of ~ 3.0 V, which can accommodate electrode materials that were otherwise forbidden in conventional aqueous electrolytes. In this study, we showed that the presence of an additive could further stabilize the aqueous electrolyte at a high voltage cathode surface. By forming a cathode electrolyte interphase (CEI) through electrochemical oxidation of tris(trimethylsilyl) borate (TMSB), we successfully stabilized LiCoO_2 in water-in-salt electrolyte at a high cut-off voltage that corresponds to 0.7e electron charge transfer. To the best of our knowledge, this is also the first electrolyte additive known to form an interphase in aqueous electrolytes. The formed CEI significantly suppressed electrolyte oxidation as well as cobalt dissolution from LiCoO_2 into electrolytes, allowing LiCoO_2 to be stably charged/discharged at a higher cut-off voltage with a high capacity utilization of 170 mA h g^{-1} . When paired with an Mo_6S_8 anode, the 2.5 V aqueous full cell delivered a high energy density of 120 W h kg^{-1} for 1000 cycles with an extremely low capacity decay rate of 0.013% per cycle.

Aqueous lithium ion batteries (ALIBs) attract intense attention due to the intrinsic non-flammable nature introduced by the aqueous electrolytes therein,^{1–4} which also makes it possible to get rid of the rigorous moisture-free manufacturing environment

Broader context

Aqueous lithium ion batteries (ALIBs) receive increasing attention due to their intrinsic non-flammable nature, which also makes it possible to get rid of the rigorous moisture-free manufacturing environment and heavy reliance on the battery management systems at module or pack levels. These characteristics make ALIBs desirable for energy storage applications. Unfortunately, ALIB development has been hindered by the low energy density. Using the "water-in-salt" electrolytes, we successfully extended the stability window of aqueous electrolyte. Hence, identifying electrodes with suitable lithiation/delithiation potentials, as well as stability, for this new class of aqueous electrolytes becomes the new challenge in maximizing the deliverable energy density of a full aqueous Li-ion battery. Herein, we stabilized LiCoO_2 at a high voltage cut-off (0.7e electron charge transfer) in a water-in-salt electrolyte by the formation of a cathode electrolyte interphase (CEI) on the LiCoO_2 surface through electrochemical oxidation of the tris(trimethylsilyl) borate additive. The high voltage LiCoO_2 cathode can provide 170 mA h g^{-1} in aqueous electrolyte. A 2.5 V aqueous full cell was thus produced and delivered with a high energy density of 120 W h kg^{-1} for 1000 cycles and an extremely low capacity decay rate of 0.013% per-cycle. The criterion for selection of the additive was also proposed, which could also be applied to other high voltage cathodes in aqueous electrolyte. The success of the additive approach in aqueous electrolytes will certainly provide a new strategy of widening voltage windows of aqueous electrolytes at low cost, eventually making it possible to develop low cost, high energy density and long cycle life aqueous batteries with intrinsic safety.

and heavy reliance on battery management systems at the module or pack levels.^{5–7} Despite these advantages, the practical application of ALIBs remains remote; primarily limited by the inferior energy density that has been imposed by the narrow electrochemical stability window of water (1.23 V).^{8–11} Recently, the electrochemical stability window of an aqueous electrolyte was shown to be able to expand significantly at high salt concentrations *via* the formation of an interphase on the anode surface and suppression of the electrochemical activity of water.¹² Such a stability window of 3.0 V (1.9–4.9 V vs. Li) provides unprecedented flexibility in selecting electrochemical couples, allowing several electrode materials that were otherwise forbidden in conventional aqueous electrolytes. Hence, identifying electrodes with suitable lithiation/delithiation potentials, as well as stability, for

^a Department of Chemical and Biomolecular Engineering, University of Maryland, College Park, MD 20742, USA. E-mail: cswang@umd.edu

^b Department of Chemical Engineering and Materials Science, Michigan State University, East Lansing, MI 48824, USA

^c Department of Nuclear Science and Engineering,

Massachusetts Institute of Technology, Cambridge, MA 02138, USA

^d Electrochemistry Branch, Sensor and Electron Devices Directorate, Power and Energy Division, U.S. Army Research Laboratory, Adelphi, MD 20783, USA

[†] Electronic supplementary information (ESI) available. See DOI: 10.1039/c6ee02604d

this new class of aqueous electrolytes becomes the new challenge in maximizing the deliverable energy density of a full aqueous Li-ion battery. While spinel-structured LiMn_2O_4 ^{13–19} suffers from poor cycling stability and olivine-structured LiFePO_4 ^{20–22} is characterized by typically low potential/low energy density, layered LiCoO_2 has been a reliable cathode material since the invention of Li-ion batteries, delivering a usable reversible capacity of $\sim 140 \text{ mA h g}^{-1}$ when charged to 4.2 V vs. Li,²³ corresponding to 50% lithium removal to $\text{Li}_{0.5}\text{CoO}_2$. This low voltage LiCoO_2 (LVLCO) has maintained the status of flagship chemistry due to its excellent cycling stability.^{24–27}

Although the lithiation/delithiation potential of LVLCO lies within the electrochemical stability window of normal aqueous electrolyte, the LVLCO still suffers from poor cycling stability due to side reactions, including the intercalation of protons into LVLCO,^{28,29} the reactions between the LVLCO and dissolved oxygen in the electrolyte,² the dissolution of Co into electrolyte³⁰ and oxygen evolution due to the oxidation of water. On the other hand, the full electrochemical stability window of water-in-salt electrolyte, with an anodic limit of 4.9 V vs. Li, is in fact not completely used by LVLCO when charged to only 4.2 V vs. Li. Recent efforts were made to charge LiCoO_2 to 4.5 V vs. Li in order to utilize more capacity from this cathode, and a capacity of $\sim 180 \text{ mA h g}^{-1}$ (corresponding to 0.7 fraction of Li removed, defined as HVLCO) was reported in organic electrolytes without structural destruction.^{23,31–35} However, the attained capacity of HVLCO gradually decays during charge/discharge cycles due to the increase in the surface impedance.²³ It was believed that both Co dissolution, along with side reactions between $\text{Li}_{0.5}\text{CoO}_2$, and electrolytes are responsible for the poor cycling stability.^{23,30,31,35} Surface coating or formation of cathode electrolyte interphases (CEI) on LiCoO_2 can effectively suppress these parasitic processes and significantly enhance the capacity retention of HVLCO.^{23,31,35} The formation of CEI was supported by the oxidative decomposition of non-aqueous solvents, which provides chemical building blocks in a similar manner as in the formation of solid electrolyte interphase (SEI) on the anode side.^{36,37} Such a chemical source is, unfortunately, absent in aqueous electrolytes, as the oxidation of either solvent (water) or salt anions cannot form a dense solid deposit on the cathode surface. Therefore, a third component responsible for interphase should be introduced. While the use of additives has been very popular in tailoring SEIs on anode surfaces recently, additives designed for cathode protection have also been reported.^{32,38–43} To our best knowledge, however, there have never been any attempts to use the additive approach in aqueous electrolyte systems.

In this work, we identified such an additive for the water-in-salt electrolyte. By electrochemical oxidation of tris(trimethylsilyl) borate (TMSB), we successfully formed a CEI on the HVLCO surface, which significantly suppressed Co-dissolution from the cathode even when 0.7 fraction of Li was removed, allowing LiCoO_2 to deliver a reversible capacity of 170 mA h g^{-1} in water-in-salt electrolytes. When coupled with an Mo_6S_8 anode, a 2.5 V aqueous full cell HVLCO/ Mo_6S_8 produces a high energy density of 120 W h kg^{-1} for 1000 cycles at an extremely low capacity decay rate of 0.013% per cycle.

The XRD pattern of pristine LiCoO_2 is shown in Fig. 1a, where all peaks can be indexed to the hexagonally packed O_3 layered structure with an $R\bar{3}m$ space group. The SEM image (Fig. 1b) reveals that all particles range between several tens of microns in size. The TEM image (Fig. 1c) confirms the typical layer structure of LiCoO_2 with a clean and well-defined surface. This cathode can be reversibly charged/discharged between 3.0 V and 4.5 V in typical non-aqueous electrolytes without severe surface structure changes,³⁵ as shown in Fig. S1 (ESI†). In water-in-salt electrolytes, the potential of redox lithiation/delithiation will shift positively by ~ 0.2 V due to the high salt concentration;¹² the corresponding upper cut-off voltage of HVLCO should be 4.7 V for the same fraction of Li removal. The galvanostatic lithiation/delithiation behavior of HVLCO in water-in-salt electrolytes was evaluated in a three-electrode cell. A reversible discharge capacity of 170 mA h g^{-1} was delivered by HVLCO when cycled between 3.2 and 4.7 V (vs. Li^+/Li) (Fig. 1d). Comparing the voltage profiles, one can easily tell that the lithiation/delithiation behavior of HVLCO in water-in-salt electrolytes is rather similar to its behavior in non-aqueous electrolytes, except for the positive potential upshift of ~ 0.2 V (Fig. S1, ESI†).

The lithiation/delithiation potential of chevrel phase Mo_6S_8 (~ 2.2 V) has been shown to rest safely within the electrochemical stability window of water-in-salt electrolytes, where it can be charged/discharged for thousands of cycles with negligible fading.¹² When coupling it with HVLCO, we produce a 2.5 V full aqueous Li-ion cell. The HVLCO/ Mo_6S_8 mass ratio was set to 1:1 in order to compensate the irreversible capacity incurred by the formation of SEI at the Mo_6S_8 anode during the initial cycles. Fig. 2a shows the charge/discharge curves of HVLCO/ Mo_6S_8 full cell between 2.5 V and 1.0 V. Two distinct voltage plateaus were observed at 0.5C for the full cell, at about 2.0 V and 1.5 V because of the two reversible redox couples of Mo_6S_8 , which are delithiated at 2.24 V and 2.67 V in water-in-salt electrolyte, respectively (Fig. S2, ESI†). A discharge capacity of 60 mA h g^{-1} (of total electrode mass) and an energy density of 120 W h kg^{-1} were obtained from such a full cell for 20 cycles, after which a rapid capacity fading occurred (Fig. 2b). However, a very stable capacity lasted for over 50 cycles when the same full cell was charged/discharged between 2.1 V and 1.0 V (Fig. S3, ESI†). The electrochemical impedance spectra (EIS) at different cycle numbers (Fig. 2c) revealed that the interfacial resistances remain stable at around 100–200 ohm during the first 20 cycles, but quickly increases to >400 ohm at the 21st cycle.

Since Mo_6S_8 has been known to stably cycle in the water-in-salt electrolyte,¹² this rapid capacity fading is highly likely to arise from the cathode side. Thus the surface structure of the cycled HVLCO was examined using HRTEM (Fig. 2d); this reveals that the smooth edges of pristine material (Fig. 1a) became rough with small notches after 50 cycles in water-in-salt electrolytes, whereas the layer structure of LiCoO_2 remained intact, as shown in the high-resolution TEM (inset of Fig. 2d & Fig. S4, ESI†). The notches on the surface of HVLCO show disordered nanocrystals with smaller d-spacing than that of LiCoO_2 , which could be indexed as cobalt oxides (Fig. S4, ESI†). We believe that the formation of a cobalt oxide layer resulted

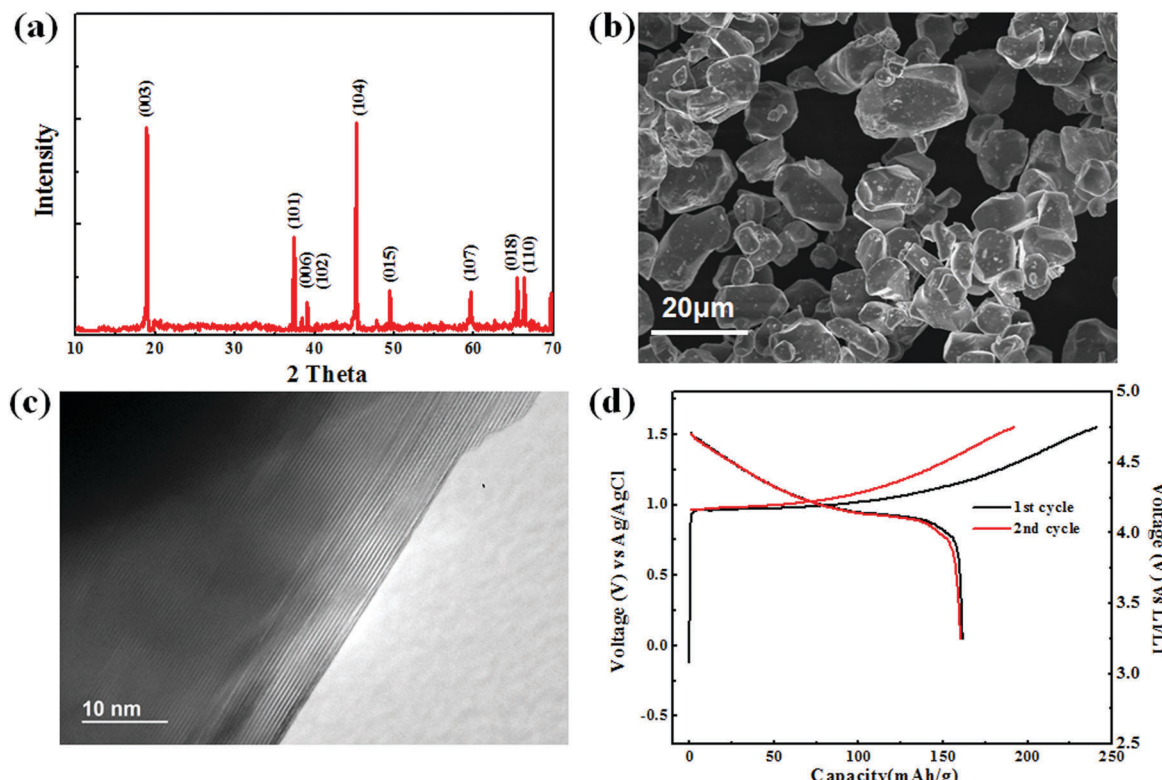


Fig. 1 (a) X-ray diffraction (XRD) pattern; (b) scanning electron microscopy (SEM) and (c) transmission electron microscopy (TEM) images of LiCoO_2 powder. (d) The typical voltage profile of LiCoO_2 between 1.5 V and 0.0 V (vs. Ag/AgCl) in water-in-salt electrolytes (21 m LiTFSI: 21 mol LiTFSI in 1 kg H_2O) at 0.2C measured in a three-electrode cell using Pt as counter and Ag/AgCl as reference electrodes.

from the reaction between the electrolyte and the HVLCO surface, which became highly oxidative with more than 0.5 fraction of Li removal. In addition, Co dissolution also occurred simultaneously, as evidenced by the inductively coupled plasma (ICP) spectroscopy analysis of the electrolyte in the HVLCO/ Mo_6S_8 full cell after 50 cycles between 2.5 V and 1.0 V (Fig. 2d inset). The concentration of the dissolved Co in the cycled electrolyte is 0.0776 ppm, and Co is not detectable in the electrolyte after 50 cycles between 2.1 V and 1.0 V. Hence, we conclude that the overall effects of both surface defects presence, Co dissolution and the formation of cobalt oxide at high voltages, are responsible for the rapid capacity fading of HVLCO in the water-in-salt electrolyte. A similar correlation among surface defects, capacity fading, and resistance growth was also established previously for LVLCO cycled in dilute aqueous electrolyte between 4.1 V and 2.7 V (vs. Li^+/Li).²⁷

The most effective and economical strategy in suppressing the damage to HVLCO surface structure and Co dissolution is to introduce extra surface protection through electrolyte additives whose electrochemical oxidation forms a solid interphase in a similar manner as the SEI formed on anode surfaces. Although the additive approach has been extensively used in non-aqueous electrolytes,⁴⁴ its application in aqueous electrolyte is hitherto unknown, and more stringent requirements have to be met in this particular case: (1) the additive itself must possess lower oxidation potential than that of the water in the water-in-salt electrolyte, which is *ca.* 4.9 V vs. Li, and (2) the additive itself must remain chemically stable against water (non-hydrolysable). After extensive

screening, we identified a borate ester, tris(trimethylsilyl) borate (TMSB), as a qualifying cathode additive, which does not hydrolyze in the water-in-salt electrolyte (Fig. S5, ESI†). This additive has also been used in non-aqueous electrolytes to form CEIs on cathodes.^{38,41} First principles calculations were carried out on TMSB, whose highest occupied molecular orbital (HOMO) level, a critical element determining oxidation reactions,⁴⁵ was compared with those of H_2O and TFSI anion in water-in-salt electrolyte. As shown in Fig. 3a, the HOMO level of TMSB is the highest among all the molecules or anions, indicating that it will be the first to be oxidized before water or salt anion when the cell voltage increases.⁴⁶ If the decomposition product is a densely-packed solid and possesses electrolyte nature, *i.e.*, ionically conductive but electronically insulating, then TMSB would serve as an excellent CEI additive in aqueous electrolyte.

To understand what TMSB will end up with, the oxidative pathway of TMSB in water was explored using the first principles calculations, whose energetically favorable oxidation pathway in water-in-salt electrolyte is shown in Fig. 3b. According to the simulation, the continuous hydrolytic reactions of oxidized TMSB (TMSB^+) will lead to the formation of boric acid and orthosilicic acid together with TMSOTMS^+ and TMSOH , which is an intermediate product. Although boric acid and orthosilicic acid dissolve in water, they are insoluble in the water-in-salt electrolyte. Thus, they could co-precipitate on the cathode surface and serve as a robust CEI. The protection mechanism of TMSB

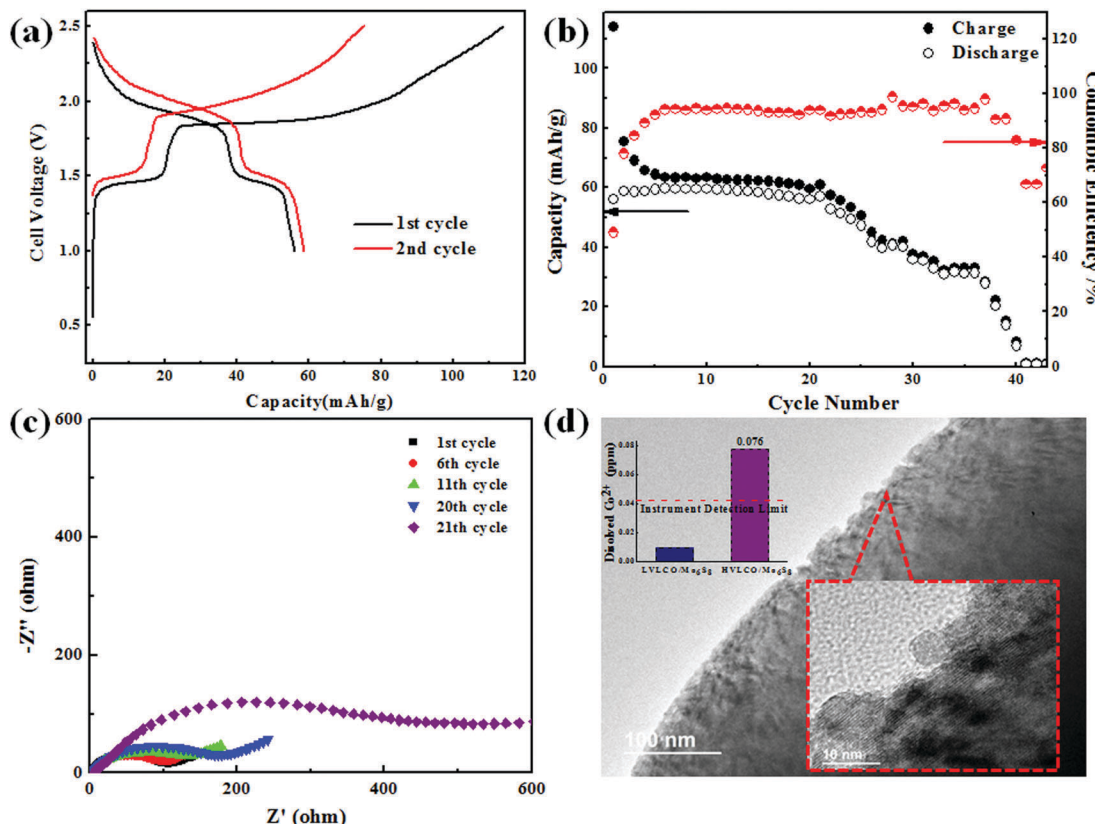


Fig. 2 The electrochemical performance of HVLCO/Mo₆S₈ full cells. (a) The typical voltage profile in water-in-salt electrolytes between 1.0 V and 2.5 V at 0.5C; (b) the cycling stability and Coulombic efficiencies at 0.5C rate; (c) electrochemical impedance spectroscopy (EIS) at the 1st, 6th, 11th, 20th, 21st cycles; (d) the TEM image for the cycled HVLCO electrodes in the 21 m LiTFSI electrolyte (inset is the amount of dissolved Co^{2+} in electrolyte measured after 50 cycles using ICP).

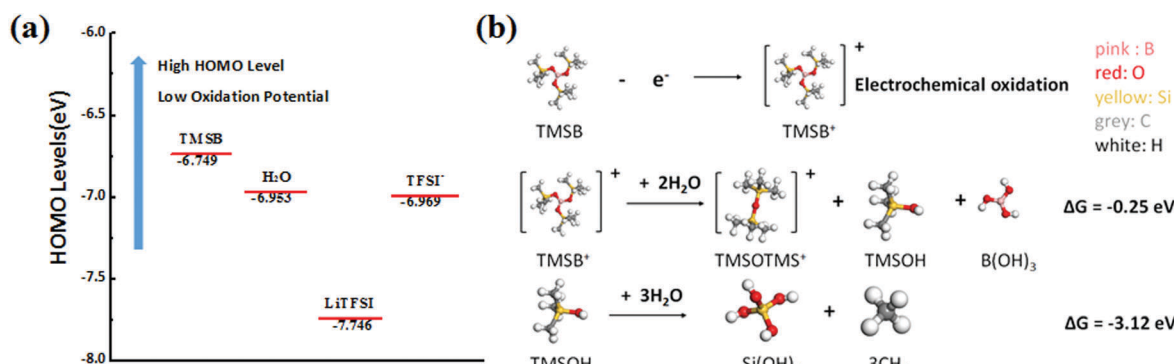


Fig. 3 (a) Highest occupied molecular orbital (HOMO) levels of TMSB, H_2O , LiTFSI and TFSI^- ; (b) schematic of possible mechanisms for electrochemical oxidative decomposition of TMSB.

additive in aqueous electrolyte should differ from TMSB in non-aqueous electrolytes. In the latter, the improved cycling performance was ascribed to the removal of HF impurity and the suppression of LiF formation.^{47,48} However, no LiF or HF should exist in our water-in-salt battery, at least not on the cathode side. On the other hand, oxygen evolution from aqueous electrolyte should become the main parasitic process that the CEI prevents.

Guided by the theoretical calculation, the galvanostatic lithiation/delithiation behavior of HVLCO was firstly evaluated

in 21 m LiTFSI electrolytes with 0.1 wt% TMSB additive using a three-electrode cell. As shown in Fig. S6 (ESI[†]), an additional plateau at ~ 1.4 V (vs. Ag/AgCl) could be observed during the first charge process, which could be ascribed to the electrochemical oxidation of TMSB. The oxidation products form an amorphous surface interphasial phase layer on the LiCoO₂ surface, as shown in Fig. S7 (ESI[†]). The coating layer significantly enhanced the cycle stability of HVLCO cathodes, as demonstrated in Fig. S8 (ESI[†]). Encouraged by the enhancement of TMSB on the cycling

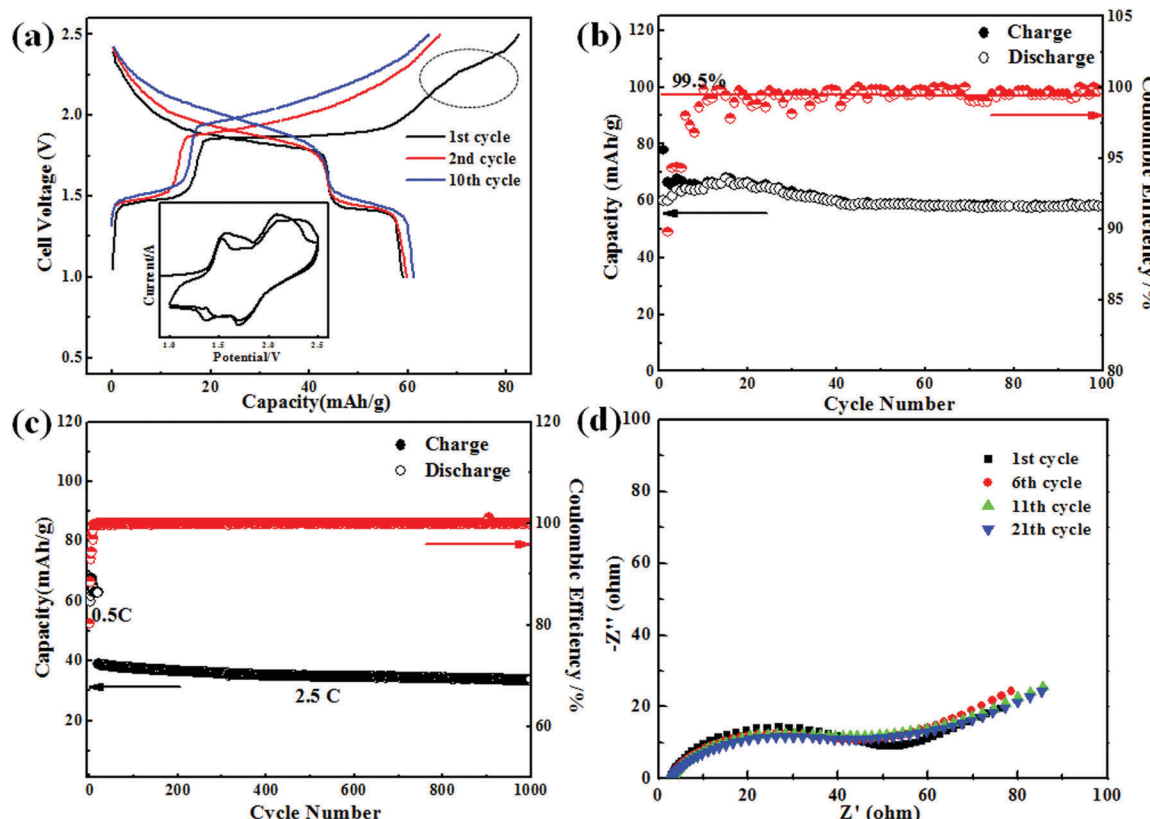


Fig. 4 The electrochemical performance of HVLCO/Mo₆S₈ full cell in 21 m LiTFSI-0.1 wt% TMSB electrolytes (a) the typical voltage profile at constant current of 0.5C between 1.0 V and 2.5 V (inset: CV curves for the HVLCO/Mo₆S₈ full cell); (b) the cycling stability and Coulombic efficiency at a low rate of 0.5C; (c) the cycling stability and coulombic efficiencies at a high rate of 2.5C after the first 20 cycles at 0.5C; (d) electrochemical impedance spectroscopy (EIS) at the 1st, 6th, 11th, 21st cycles.

stability of HVLCO cathode, a HVLCO/Mo₆S₈ full cell was thus assembled and evaluated in the 21 m LiTFSI-0.1 wt% TMSB electrolytes. Fig. 4a shows the charge/discharge behavior of the full cell at the 0.5C rate. In the first charge, an additional plateau (highlighted by a circle) was observed due to the TMSB oxidation. After the first charging, the following voltage profiles become identical to those of HVLCO/Mo₆S₈ full cell in additive-free electrolytes, suggesting that TMSB does not affect the electrochemical lithiation/delithiation of both HVLCO cathode or Mo₆S₈ anode, except for the 1st cycle where CEI forms on the HVLCO surface.

The oxidation of TMSB must have formed a stable surface interphasial phase, which significantly suppressed parasitic reactions on the highly oxidizing HVLCO surface, because the columbic efficiency increased from 94% of TMSB-free electrolyte (Fig. 2b) to nearly ~100% in the 21 m LiTFSI-0.1 wt% TMSB electrolyte (Fig. 4b) after just the first 8 cycles. Moreover, the irreversible capacity induced by formation of CEI on HVLCO cathode in the first charge, which should produce extra Li⁺, was cancelled out by the negative irreversible capacity from formation of an SEI on Mo₆S₈ anode, which consumes Li⁺. The net result is that the columbic efficiency in the first cycle improved from 50% of TMSB-free electrolyte (Fig. 2b) to 75% in the 21 m LiTFSI-0.1 wt% TMSB electrolyte (Fig. 4b). Remarkably, 92% capacity retention was achieved for the full cell after 100 cycles

at 0.5C rate. The long term cycling stability of the HVLCO/Mo₆S₈ full cell was examined at a high rate of 2.5C (Fig. 4c), where extremely high capacity retention with a minimum capacity decay rate of 0.013% per cycle was observed for 1000 cycles in the 21 m LiTFSI-0.1 wt% TMSB electrolyte. The stable interfacial impedance as detected by EIS at different cycles (Fig. 4d) confirmed the effective protection of CEI on the HVLCO surface. At a rate of 0.5C the HVLCO/Mo₆S₈ full cell using 21 m LiTFSI-0.1 wt% TMSB electrolytes provides an energy density of 120 W h kg⁻¹, which is among the highest energy density in all the aqueous batteries reported to date (Fig. S9, ESI†).

The chemical composition of CEI on the HVLCO surface formed by the oxidation of TMSB additive was analyzed by TEM. Fig. 5a and 5b show the surface morphology of the HVLCO electrode after 100 charge/discharge cycles in the electrolytes with TMSB additive. A ~10 nm thick conformal coating layer is observed on an HVLCO particle, which is attributed to the electrochemical oxidation of TMSB additive during the charging process. The HRTEM image (Fig. 5b) further reveals the amorphous nature of the surface coating layer. In contrast with Fig. 2d, no evident surface defects were observed on the HVLCO that was now protected by the CEI, suggesting that the surface layer eliminates Co dissolution and hence improves the cycle performance of HVLCO. The suppression of Co dissolution was also confirmed by the ICP analysis

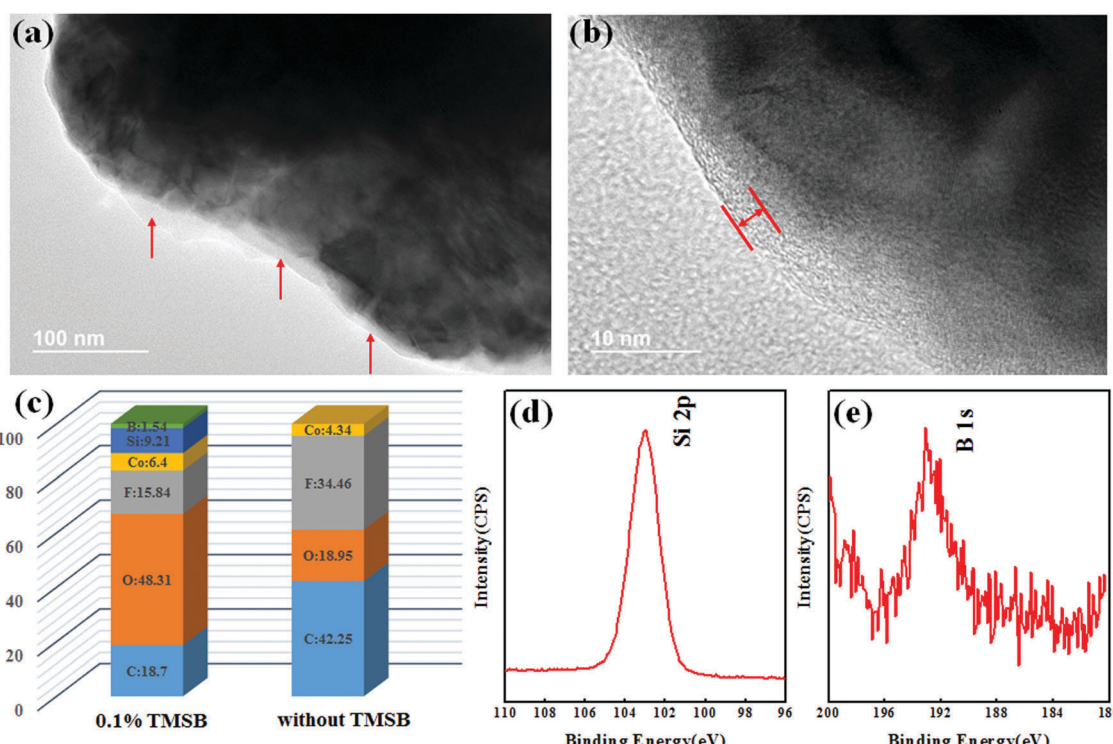


Fig. 5 (a) and (b) The TEM image for the HVLCO electrodes after cycling in 21 m LiTFSI-0.1 wt% TMSB electrolytes; (c) atomic compositions of the surface films on HVLCO electrodes after cycling; XPS spectra for (d) Si_{2p} and (e) B_{1s} on the surface of the HVLCO electrode after cycling in 21 m LiTFSI-0.1 wt% TMSB electrolytes.

(Fig. S10, ESI†), where the concentration of dissolved Co in electrolytes with TMSB additive after 100 cycles was negligible. The HVLCO retains the original layered structure after the 100 charge/discharge cycles, as demonstrated by the *ex situ* XRD (Fig. S11, ESI†).

The composition of CEI was determined using XPS by examining the surfaces of the cycled HVLCO cathode with and without TMSB additive. The atomic compositions of the surface layer are listed in Fig. 5c. Compared with the surface composition of HVLCO cycled in additive-free water-in-salt electrolyte; additional signals corresponding to Si (Si_{2p}) and B (B_{1s}) elements are clearly detected on the surface of HVLCO cycled in the presence of 0.1 wt% TMSB (Fig. 5d and e). The binding energy of Si_{2p} is located at ~103 eV, between the Si⁴⁺ (103.4 eV) and Si³⁺ (102.1 eV).⁴⁹ Therefore, we assign it to the species of Si(OH)₄ containing minor fractions of Si(OH)₃. Similarly, the binding energy peak of B_{1s} at 193 eV is attributed to the B(OH)₃ with minor boron subhydroxides,⁵⁰ which is in agreement with the simulation results in Fig. 3b. All these electrochemical, surface analysis and first principle calculations converge to suggest that TMSB additive in water-in-salt electrolytes can form protective CEI on the HVLCO surface, thus allowing HVLCO to be stably charged/discharged at a high cut-off voltage, delivering a high capacity of 170 mA h g⁻¹ with excellent stability for 1000 cycles. What is more important than the achieved energy density and cycling stability, is the fact that the interphasial additive approach works in aqueous electrolyte. This new finding opens up a new strategy to enhance energy density and cycle life of aqueous electrolyte Li-ion batteries.

Conclusions

We have demonstrated that the high voltage LiCoO₂ can provide a high capacity of 170 mA h g⁻¹ with exceptional cycling stability in water-in-salt electrolytes when its surface is protected by an interphase formed by an additive. Paired with a Mo₆S₈ anode, the 2.5 V HVLCO/Mo₆S₈ aqueous full cell delivered a high energy density of 120 W h kg⁻¹ for 1000 cycles with an extremely low capacity decay rate of 0.013% per cycle, which is among the highest energy density and longest cycle stability in all aqueous Li-ion batteries reported to date. The XPS and the first principles calculation demonstrated that TMSB additive was electrochemically oxidized and formed a densely-packed CEI on the surface of the HVLCO, preventing Co dissolution and other parasitic reactions between HVLCO and electrolytes. The screening process could also be extended to other choices. For example, thiophene (HOMO level: -5.8 eV) could also form the CEI through the electrochemical oxidative polymerization process (Fig. S12, ESI†). The success of the additive approach in aqueous electrolytes will provide a new strategy for developing high energy density and long cycle life aqueous Li-ion batteries with intrinsic safety.

Experimental

Materials

Lithium bis(trifluoromethane sulfonyl) imide (LiN(SO₂CF₃)₂, LiTFSI) (> 98%) and water (HPLC grade) were purchased from Tokyo Chemical Industry and Sigma-Aldrich, respectively. The water-in-salt electrolyte (21 m LiTFSI) is prepared by dissolving

LiTFSI in water according to molality (21 mol salt in 1 kg water). The tris(trimethylsilyl) borate (TMSB) was purchased from Sigma-Aldrich. 0.1% mass ration of TMSB additive was added to the water-in-salt electrolyte to form the 21 m LiTFSI-0.1 wt% TMSB electrolyte.

The LiCoO₂ materials were purchased from MTI Corporation. Chevrel phase Mo₆S₈ was prepared according to previous reports.

Materials characterizations

The morphology of the sample was investigated by scanning electron microscopy (SEM, Hitachi SU-70) and transmission electron microscopy (TEM, JEM 2100 FEG, 200 keV). All the samples for *ex situ* TEM were recovered from full aqueous Li-ion battery in 2032 coin cell configuration after electrochemical cycling. The samples were washed by DME three times and then dried under vacuum for two hours. X-ray diffraction (XRD) patterns were obtained on a Bruker Smart 1000 (Bruker AXS, Inc.) using Cu-K α radiation with an airtight holder from Bruker. X-ray photoelectron spectroscopy (XPS) was conducted on a high sensitivity Kratos AXIS 165 X-ray photoelectron spectrometer with Mg-K α radiation. For ICP measurements, the electrolyte for the full aqueous Li-ion battery with 3 mg cathode assembled in a bottle was diluted in 2% HNO₃ solution to form 25 mL solution. ICP-OES measurements were performed using a Shimadzu ICPE-9820 Dual View Spectrometer.

Electrochemical measurements

The LiCoO₂ and Mo₆S₈ electrodes were fabricated by compressing active materials, carbon black, and Polytetrafluoroethylene (PTFE) at a weight ratio of 8:1:1 onto the titanium mesh and the stainless steel grid, respectively. The three-electrode devices for cathode consists of LiCoO₂ composite (about 2 mg) as working, active carbon as the counter and Ag/AgCl as the reference electrode. Cyclic voltammetry (CV) was carried out using a CHI 600E electrochemical work station at scanning rate of 0.1 mV s⁻¹ for these composite working electrodes. The potentials *vs.* Ag/AgCl were converted to those *vs.* standard Li⁺/Li, supposing that the potential of Ag/AgCl electrode was 3.239 V *vs.* Li⁺/Li.

The full ALIB cell was assembled in CR2032-type coin cell using LiCoO₂ cathode (about 10 mg cm⁻²), Mo₆S₈ anode (about 8 mg cm⁻²) and glass fiber as separator. The charge-discharge experiments were performed on a Land BT2000 battery test system (Wuhan, China) at room-temperature.

DFT calculation

All electron DFT calculations with unrestricted spin were conducted under Dmol3 modules in Materials Studio within GGA PW91 functional. 3.5 version Double Numerical plus *d*-functions (DND) basis set was chosen. Conductor-like screening model (COSMO), in which solvent is approximated by a dielectric continuum surrounding the solute molecules outside of a molecular cavity, is used to investigate the influence of water solvent and the dielectric constant of water (78.54) was applied. To ensure the configuration of lowest energy, geometry optimization was conducted with several different initial configurations and the optimized configuration with lowest energy was selected.

Acknowledgements

The authors gratefully acknowledge funding support from DOE ARPA-E (DEAR0000389). We also acknowledge the support of the Maryland Nano Center and its NispLab. The NispLab is supported in part by the NSF as a MRSEC Shared Experimental Facility. YXL, YQ, and CSW acknowledge the support for the computational work as part of the Nanostructures for Electrical Energy Storage (NEES), an Energy Frontier Research Center funded by the U.S. Department of Energy, Office of Science, Basic Energy Sciences under Award number DESC0001160.

References

- 1 W. Li, J. R. Dahn and D. S. Wainwright, *Science*, 1994, **264**, 1115–1118.
- 2 J.-Y. Luo, W.-J. Cui, P. He and Y.-Y. Xia, *Nat. Chem.*, 2010, **2**, 760–765.
- 3 H. Kim, J. Hong, K.-Y. Park, H. Kim, S.-W. Kim and K. Kang, *Chem. Rev.*, 2014, **114**, 11788–11827.
- 4 W. Tang, Y. S. Zhu, Y. Y. Hou, L. L. Liu, Y. P. Wu, K. P. Loh, H. P. Zhang and K. Zhu, *Energy Environ. Sci.*, 2013, **6**, 2093–2104.
- 5 B. Dunn, H. Kamath and J.-M. Tarascon, *Science*, 2011, **334**, 928–935.
- 6 J. B. Goodenough and Y. Kim, *Chem. Mater.*, 2010, **22**, 587–603.
- 7 M. Armand and J. M. Tarascon, *Nature*, 2008, **451**, 652–657.
- 8 S. F. Lux, L. Terborg, O. Hachmoeller, T. Placke, H. W. Meyer, S. Passerini, M. Winter and S. Nowak, *J. Electrochem. Soc.*, 2013, **160**, A1694–A1700.
- 9 M. S. Hong, S. H. Lee and S. W. Kim, *Electrochem. Solid-State Lett.*, 2002, **5**, A227.
- 10 D. Gordon, M. Y. Wu, A. Ramanujapuram, J. Benson, J. T. Lee, A. Magasinski, N. Nitta, C. Huang and G. Yushin, *Adv. Energy Mater.*, 2016, **6**, 1501805.
- 11 D. W. McOwen, D. M. Seo, O. Borodin, J. Vatamanu, P. D. Boyle and W. A. Henderson, *Energy Environ. Sci.*, 2014, **7**, 416–426.
- 12 L. Suo, O. Borodin, T. Gao, M. Olguin, J. Ho, X. Fan, C. Luo, C. Wang and K. Xu, *Science*, 2015, **350**, 938–943.
- 13 W. Tang, L. L. Liu, Y. S. Zhu, H. Sun, Y. P. Wu and K. Zhu, *Energy Environ. Sci.*, 2012, **5**, 6909–6913.
- 14 J.-Y. Luo and Y.-Y. Xia, *Adv. Funct. Mater.*, 2007, **17**, 3877–3884.
- 15 J. Yan, J. Wang, H. Liu, Z. Bakenov, D. Gosselink and P. Chen, *J. Power Sources*, 2012, **216**, 222–226.
- 16 S. Liu, S. H. Ye, C. Z. Li, G. L. Pan and X. P. Gao, *J. Electrochem. Soc.*, 2011, **158**, A1490.
- 17 Y. G. Wang and Y. Y. Xia, *Electrochim. Commun.*, 2005, **7**, 1138–1142.
- 18 H. Wang, Y. Zeng, K. Huang, S. Liu and L. Chen, *Electrochim. Acta*, 2007, **52**, 5102–5107.
- 19 Q. T. Qu, L. J. Fu, X. Y. Zhan, D. Samuelis, J. Maier, L. Li, S. Tian, Z. H. Li and Y. P. Wu, *Energy Environ. Sci.*, 2011, **4**, 3985–3990.

- 20 M. Manickam, P. Singh, S. Thurgate and K. Prince, *J. Power Sources*, 2006, **158**, 646–649.
- 21 P. He, J.-L. Liu, W.-J. Cui, J.-Y. Luo and Y.-Y. Xia, *Electrochim. Acta*, 2011, **56**, 2351–2357.
- 22 Y. Y. Hou, X. J. Wang, Y. S. Zhu, C. L. Hu, Z. Chang, Y. P. Wu and R. Holze, *J. Mater. Chem. A*, 2013, **1**, 14713–14718.
- 23 Z. Chen and J. R. Dahn, *Electrochim. Acta*, 2004, **49**, 1079–1090.
- 24 R. Ruffo, F. La Mantia, C. Wessells, R. A. Huggins and Y. Cui, *Solid State Ionics*, 2011, **192**, 289–292.
- 25 G. J. Wang, Q. T. Qu, B. Wang, Y. Shi, S. Tian, Y. P. Wu and R. Holze, *Electrochim. Acta*, 2009, **54**, 1199–1203.
- 26 R. Ruffo, C. Wessells, R. A. Huggins and Y. Cui, *Electrochem. Commun.*, 2009, **11**, 247–249.
- 27 A. Ramanujapuram, D. Gordon, A. Magasinski, B. Ward, N. Nitta, C. Huang and G. Yushin, *Energy Environ. Sci.*, 2016, **9**, 1841–1848.
- 28 X. Gu, J.-l. Liu, J.-h. Yang, H.-j. Xiang, X.-g. Gong and Y.-y. Xia, *J. Phys. Chem. C*, 2011, **115**, 12672–12676.
- 29 J. Choi, E. Alvarez, T. A. Arunkumar and A. Manthiram, *Electrochim. Solid-State Lett.*, 2006, **9**, A241–A244.
- 30 D. Aurbach, B. Markovsky, A. Rodkin, E. Levi, Y. S. Cohen, H. J. Kim and M. Schmidt, *Electrochim. Acta*, 2002, **47**, 4291–4306.
- 31 Y. Sun, J. Han, S. Myung, S. Lee and K. Amine, *Electrochem. Commun.*, 2006, **8**, 821–826.
- 32 J.-N. Lee, G.-B. Han, M.-H. Ryou, D. J. Lee, S. Jongchan, J. W. Choi and J.-K. Park, *Electrochim. Acta*, 2011, **56**, 5195–5200.
- 33 F. Zhao, Y. Tang, J. Wang, J. Tian, H. Ge and B. Wang, *Electrochim. Acta*, 2015, **174**, 384–390.
- 34 X. Dai, A. Zhou, J. Xu, Y. Lu, L. Wang, C. Fan and J. Li, *J. Phys. Chem. C*, 2016, **120**, 422–430.
- 35 H. Xia, L. Lu, Y. S. Meng and G. Ceder, *J. Electrochem. Soc.*, 2007, **154**, A337.
- 36 M. Gauthier, T. J. Carney, A. Grimaud, L. Giordano, N. Pour, H. H. Chang, D. P. Fenning, S. F. Lux, O. Paschos, C. Bauer, F. Maglia, S. Lupart, P. Lamp and Y. Shao-Horn, *J. Phys. Chem. Lett.*, 2015, **6**, 4653–4672.
- 37 K. Xu, *Chem. Rev.*, 2014, **114**, 11503–11618.
- 38 X. Zuo, C. Fan, J. Liu, X. Xiao, J. Wu and J. Nan, *J. Power Sources*, 2013, **229**, 308–312.
- 39 A. von Cresce and K. Xu, *J. Electrochem. Soc.*, 2011, **158**, A337.
- 40 L. Xia, Y. Xia and Z. Liu, *Electrochim. Acta*, 2015, **151**, 429–436.
- 41 H. Rong, M. Xu, B. Xie, X. Liao, W. Huang, L. Xing and W. Li, *Electrochim. Acta*, 2014, **147**, 31–39.
- 42 S. Tan, Z. Zhang, Y. Li, Y. Li, J. Zheng, Z. Zhou and Y. Yang, *J. Electrochim. Soc.*, 2012, **160**, A285–A292.
- 43 Y. Liu, L. Tan and L. Li, *J. Power Sources*, 2013, **221**, 90–96.
- 44 K. Xu, *Chem. Rev.*, 2004, **104**, 4303–4418.
- 45 Y. K. Han, J. Yoo and T. Yim, *J. Mater. Chem. A*, 2015, **3**, 10900–10909.
- 46 X. L. Liao, P. Y. Sun, M. Q. Xu, L. D. Xing, Y. H. Liao, L. P. Zhang, L. Yu, W. Z. Fan and W. S. Li, *Appl. Energy*, 2016, **175**, 505–511.
- 47 J. H. Li, L. D. Xing, R. Q. Zhang, M. Chen, Z. S. Wang, M. Q. Xu and W. S. Li, *J. Power Sources*, 2015, **285**, 360–366.
- 48 Y. M. Song, J. G. Han, S. Park, K. T. Lee and N. S. Choi, *J. Mater. Chem. A*, 2014, **2**, 9506–9513.
- 49 J. W. He, X. Xu, J. S. Corneille and D. W. Goodman, *Surf. Sci.*, 1992, **279**, 119–126.
- 50 Y. J. Wang, J. F. Fan and M. Trenary, *Chem. Mater.*, 1993, **5**, 192–198.